Article:
Song, K.W. and Kyriienko, O. (2025) Electrically tunable and enhanced nonlinearity of moiré exciton polaritons in transition metal dichalcogenide bilayers. Physical Review Letters, 135 (3). 036901. ISSN: 0031-9007

https://doi.org/10.1103/gr72-szwg

Electrically Tunable and Enhanced Nonlinearity of Moiré Exciton Polaritons in Transition Metal Dichalcogenide Bilayers

Kok Wee Song[1,2] and Oleksandr Kyriienko[1,3]
[1]Department of Physics and Astronomy, University of Exeter, Stocker Road, Exeter EX4 4QL, United Kingdom
[2]Department of Physics, Xiamen University of Malaysia, 43900 Sepang, Malaysia
[3]School of Mathematical and Physical Sciences, University of Sheffield, Sheffield S10 2TN, United Kingdom

(Received 21 June 2024; accepted 23 June 2025; published 15 July 2025)

We develop a microscopic theory for nonlinear optical response of moiré exciton polaritons in bilayers of transition metal dichalcogenides (TMDs). Our theory allows us to study the tunnel-coupled intralayer and interlayer excitonic modes for a wide range of twist angles (θ), external electric field, and light-matter coupling, providing insights into the hybridization regime inaccessible before. Specifically, we account for the umklapp scattering processes of two exciton polaritons responsible for enhanced nonlinearity, and show that it is crucial for describing interactions at strong hybridization. We reveal a regime of attractive nonlinearity for moiré polaritons, stemming from the anisotropic Coulomb interactions, which can explain some of experimental features of optical response in TMD bilayers. Furthermore, within our theory we demonstrate that the attractive nonlinearity can be tuned into repulsive by applying an external electric field. Our findings show that nonlinear moiré polaritons offer a controllable platform nonlinear polaritonic devices.

DOI: 10.1103/gr72-szwg

Introduction—Moiré superlattices formed in twisted bilayers of atomically thin crystals represent a unique platform for studying strongly correlated physics [1–3], with emergent superconductivity in moiré bilayers of graphene serving as a prominent example [4]. The essence of moiré engineering is to generate the band mixing between monolayer crystals by forming a moiré pattern with reduced crystal translational symmetry. At small twist angles, as the folded band energies come closer together, the interlayer tunneling induces a strong band hybridization that profoundly changes low energy states of materials, manifested in flatbands and unique transport properties [5–7]. Moiré engineering is also an effective tool for tuning the optical properties [8–11]. This was demonstrated in TMD bilayers, revealing their stacking- and twist-dependent optics [12–17].

Moiré excitons, represented by electron-hole bound states spread over several layers of material, lead to a pronounced optical response of 2D bilayers [18,19], and offer a platform for quantum optical applications [20,21]. Their linear properties demonstrate a dipolar response and electrical tunability [22–26]. Similar hybridized intra–interlayer excitons appear in homobilayer systems for selected stacking [27–30]. When embedded into a microcavity, hybridized moiré excitons can couple strongly to photons and form polaritons [30–32]. Nonlinear optical response of hybridized excitons and polaritons in TMDs revealed enhancement as compared to the monolayer response [30–34] and suggested electric field dependence [35,36]. The presence of nonlinearity is important for the emergence of exotic correlated phases [37–41] and underpins strong photonic nonlinearity [31,42,43] important for driving the system into a quantum regime [44–46]. However, despite significant advances, the theoretical description of nonlinear interaction for hybridized moiré-type excitons and polaritons has been limited to specific stackings (thus not twist-dependent), considering simplified mode wave functions, and treating fixed (top-bottom) excitonic configurations.

In this Letter, we develop a microscopic theory of twisting-dependent optical response of 2D bilayers, taking into account a rich structure of moiré modes. Solving a Wannier equation within the multi-Gaussian basis expansion, we resolve excitonic modes emerging from hybridization of interlayer and intralayer states at varying twisting angles and external bias. Crucially, this allows calculating nonlinear scattering for different modes without simplifying their structure, as well as describing strong light-matter coupling. We observe that the umklapp scattering involving neighboring mini Brillouin zones (mBZ) of the moiré lattice play an important role for nonlinearity, leading to its enhancement for nonzero θ. For bilayers with small

twisting we reveal an attractive nonlinearity driven by exchange processes, and recover a conventional dipolar repulsion for large ($> 3°$) twists. Our results can offer microscopic insights into nonlinear redshifts measured experimentally [30,47], and open avenues for quantitative studies of quantum moiré polaritons.

Model—We consider a bilayer Hamiltonian $\mathcal{H} = \mathcal{H}_0 + \mathcal{H}_{\rm int} + \mathcal{H}_t$, consisting of the free energy terms, Coulomb interaction term, and the tunneling term, respectively. The free energy for electrons (e) and hole (h) in different layers reads as $\mathcal{H}_0 = \sum_{\mathbf{k}\sigma}\sum_{\ell=1,2}[\varepsilon^c_{\ell\sigma}(\mathbf{k}) a^{\ell,\dagger}_{\mathbf{k}\sigma} a^{\ell}_{\mathbf{k}\sigma} + \varepsilon^v_{\ell\sigma}(\mathbf{k}) b^{\ell,\dagger}_{\mathbf{k}\sigma} b^{\ell}_{\mathbf{k}\sigma}]$, where a crystal momentum $\mathbf{k}$ is measured from the Γ point in each layer labeled as $\ell = 1$, 2, and $\sigma = \uparrow, \downarrow$ is the spin index. The density-density interaction term reads $\mathcal{H}_{\rm int} = (1/2L^2)\sum_{\ell\ell',\mathbf{q}} v_{\ell\ell'}(\mathbf{q})\rho_{\ell\mathbf{q}}\rho_{\ell',-\mathbf{q}}$, where L^2 is a sample area. Since only the low-energy e-h pairs are relevant for forming the exciton-bound state [48,49], we expand the dispersion near the valleys at $\mathbf{K}_\ell$ (band edge) as $\varepsilon^{\rm b}_{\ell\sigma}(\mathbf{k}) = \Delta^{\rm b}_{\ell\sigma} \pm (\mathbf{k} - \mathbf{K}_\ell)^2/(2m^{\rm b}_\ell)$ with ${\rm b} = c, v$ being the conduction and valence band index, and $m^{\rm b}_\ell$ being the b-band mass in layer ℓ. We let the energy offset for the b-band edge as $\Delta^{\rm b}_{\ell\sigma}$ that is measured from the topmost valence band [see Fig. 1(c)]. In the Coulomb term, $\rho_{\ell\mathbf{q}} = \sum_{\mathbf{k}\sigma}(a^{\ell\dagger}_{\mathbf{k}+\mathbf{q},\sigma} a^{\ell}_{\mathbf{k}\sigma} + b^{\ell\dagger}_{\mathbf{k}+\mathbf{q},\sigma} b^{\ell}_{\mathbf{k}\sigma})$ is the charge density, operator, and the screened potential between electrons is of the Keldysh-Rytova form [50],

$$v_{\ell\ell'}(\mathbf{q}) = \frac{2\pi}{\epsilon q}\frac{\kappa_{\ell\ell'}(q)}{(1 + r_1 q)(1 + r_2 q) - r_1 r_2 q^2 {\rm e}^{-2qd}}, \quad (1)$$

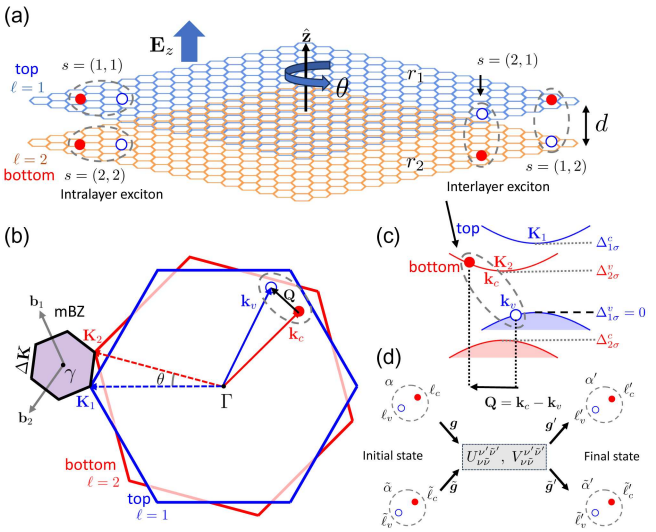

FIG. 1. (a) Sketch of a bilayer system, showing two types of interlayer and intralayer excitons. (b) Brillouin zones of top (blue) and bottom (red) monolayer. Mini Brillouin zones (mBZ) of the moiré bilayer. (c) Sketch of interlayer exciton in momentum space. (d) Diagram of exciton-exciton Coulomb interaction where electron and hole layer indices ℓ do not change, and same-layer identical particles can be exchanged.

where ϵ is the dielectric constant of the environment, r_ℓ is the screening length of the material, and d is the interlayer distance [see Fig. 1(a)]. Here, $\kappa_{12}(q) = \kappa_{21}(q) = {\rm e}^{-qd}$, $\kappa_{11}(q) = 1 + r_2 q(1 - {\rm e}^{-2qd})$, and $\kappa_{22}(q) = 1 + r_1 q(1 - {\rm e}^{-2qd})$. The interlayer hopping Hamiltonian in the continuum limit reads as

$$\mathcal{H}_t = \sum_{\ell\ell'}\sum_{\mathbf{k}\mathbf{k}'}\left[T^c_{\ell'\ell}(\mathbf{k}', \mathbf{k}) a^{\ell',\dagger}_{\mathbf{k}'\sigma} a^{\ell}_{\mathbf{k}\sigma} + T^v_{\ell'\ell}(\mathbf{k}', \mathbf{k}) b^{\ell',\dagger}_{\mathbf{k}'\sigma} b^{\ell}_{\mathbf{k}\sigma}\right] \quad (2)$$

with interband hoppings being omitted [51].

Exciton bound states—The Coulomb interaction described by $\mathcal{H}_{\rm int}$ gives rise to an exciton bound state described by a linear combination

$$X^{s\dagger}_{\alpha\sigma}(\mathbf{Q}) = \sum_{\mathbf{k}_c,\mathbf{k}_v}\delta_{\mathbf{k}_c - \mathbf{k}_v, \mathbf{Q}}\phi^s_{\alpha\sigma}(\mathbf{p}) a^{\ell_c\dagger}_{\mathbf{k}_c\sigma} b^{\ell_v}_{\mathbf{k}_v\sigma}, \quad (3)$$

where α is the exciton principal quantum number, and excitonic wave function is described by separated variables corresponding to the center-of-mass motion with total momentum $\mathbf{Q} = \mathbf{k}_c - \mathbf{k}_v$, and the relative motion with momentum $\mathbf{p} = [m^v_{\ell_v}(\mathbf{k}_c - \mathbf{K}_{\ell_c}) + m^c_{\ell_c}(\mathbf{k}_v - \mathbf{K}_{\ell_v})]/(m^c_{\ell_c} + m^v_{\ell_v})$. Here, $s = (\ell_c, \ell_v)$ is the double index labeling the exciton species [intralayer or interlayer, see Fig. 1(a)]. The relative motion wave function satisfies the Wannier equation

$$\left[\frac{\mathbf{p}^2}{2\mu_s} + \frac{(\mathbf{Q} - \Delta\mathbf{K})^2}{2M_s} + \varepsilon^s_\sigma\right]\phi^s_{\alpha\sigma}(\mathbf{p}) - \sum_{\mathbf{q}} v_s(\mathbf{q})\phi^s_{\alpha\sigma}(\mathbf{p} + \mathbf{q}) = E^s_{\alpha\sigma}(\mathbf{Q})\phi^s_{\alpha\sigma}(\mathbf{p}), \quad (4)$$

with $\Delta\mathbf{K} = \mathbf{K}_{\ell_c} - \mathbf{K}_{\ell_v}$, $\varepsilon^s_\sigma = \Delta^c_{\ell_c\sigma} - \Delta^v_{\ell_v\sigma}$, and $E^s_{\alpha\sigma}(\mathbf{Q})$ being the exciton energy. The total mass and reduced mass are $M_s = m^c_{\ell_c} + m^v_{\ell_v}$, and $\mu_s = m^c_{\ell_c} m^v_{\ell_v}/M_s$.

Hybridized moiré exciton—Because of the interlayer hopping, the exciton in the moiré bilayer becomes a hybridized state between different excitonic modes in Eq. (3) with $(s, \alpha, \mathbf{Q})$. To find the *hybridized* moiré exciton, we approximate the interlayer hopping constant in the vicinity of the valleys $\mathbf{K}_\ell$ in both layers as [51,52]

$$T^{c,v}_{\ell'\ell}(\mathbf{k}', \mathbf{k}) = \sum_{\mathbf{G}_\ell\mathbf{G}_{\ell'}} t^{c,v}(\mathbf{K}_\ell + \mathbf{G}_\ell)\delta_{\mathbf{k}'-\mathbf{k}, \mathbf{G}_{\ell'} - \mathbf{G}_\ell}\tau^x_{\ell\ell'}, \quad (5)$$

where $\mathbf{G}_\ell$ is the monolayer reciprocal lattice vector in layer ℓ. The matrix $\tau^x_{11} = \tau^x_{22} = 0$ and $\tau^x_{12} = \tau^x_{21} = 1$. This interlayer scattering reduces the translational crystal symmetry of the monolayer lattice into the moiré superlattice. As indicated by the delta function in Eq. (5), this scattering preserved the momentum up to $\mathbf{G}_\ell - \mathbf{G}_{\ell'} = i\mathbf{b}_1 + j\mathbf{b}_2$ where i, j are integers and $\mathbf{b}_{1,2}$ are the primitive reciprocal

lattice vectors of the moiré bilayer [52] [see Fig. 1(b)]. As a result, the momentum within the moiré mini Brillouin zone $\bar{\mathbf{Q}}$ is a conserved quantity. Therefore, this $\bar{\mathbf{Q}}$-preserving interlayer scattering leads to the formation of a *hybridized* moiré exciton as

$$\mathcal{X}^{\bar{\alpha}\dagger}_{\sigma}(\bar{\mathbf{Q}}) = \sum_{\nu} C^{\bar{\alpha}}_{\nu\sigma}(\bar{\mathbf{Q}}) X^{\dagger}_{\nu\sigma}(\bar{\mathbf{Q}}), \tag{6}$$

where we have used the shorthand index $\nu = (s, \alpha, \boldsymbol{g})$ to represent exciton species s, exciton state α, and reciprocal lattice vector $\boldsymbol{g} = i\mathbf{b}_1 + j\mathbf{b}_2$ to lighten our notation [Fig. 1(d)]. Also, we let $X^{\dagger}_{\nu\sigma}(\bar{\mathbf{Q}}) = X^{s\dagger}_{\alpha\sigma}(\bar{\mathbf{Q}} + \boldsymbol{g})$. The *hybridized* moiré exciton can be obtained by solving

$$[E_{\nu\sigma}(\bar{\mathbf{Q}}) - \mathcal{E}^{\bar{\alpha}}_{\sigma}(\bar{\mathbf{Q}})] C^{\bar{\alpha}}_{\nu\sigma}(\bar{\mathbf{Q}}) = \sum_{\nu'} w_{\nu'\nu}(\bar{\mathbf{Q}}) C^{\bar{\alpha}}_{\nu'\sigma}(\bar{\mathbf{Q}}), \tag{7}$$

where $E_{\nu\sigma}(\bar{\mathbf{Q}}) = E^{s}_{\alpha\sigma}(\bar{\mathbf{Q}} + \boldsymbol{g})$, and the interlayer-to-intralayer exciton transition matrix elements is

$$\langle 0 | X_{\nu'}(\bar{\mathbf{Q}}') \mathcal{H}_t X^{\dagger}_{\nu}(\bar{\mathbf{Q}}) | 0 \rangle = w_{\nu'\nu}(\bar{\mathbf{Q}}) \delta_{\bar{\mathbf{Q}}',\bar{\mathbf{Q}}}, \tag{8}$$

with $|0\rangle$ being the ground state. In Eq. (7), we label the *hybridized* moiré exciton eigenstates by index $\bar{\alpha}$ with a bar, see details in Supplemental Material [53]. The excitonic model here is different from the moiré potential approach [5,8,41], which does not account for the interlayer–intralayer exciton hybridization.

Exciton-exciton interaction—In our analysis we go beyond single-particle properties and study correlation effects for moiré excitons arising from their interactions. We concentrate on $1s$ states ($\alpha = 0$) and set $\bar{\mathbf{Q}} = 0$ in the scattering processes, such that we characterize the low-energy exciton-exciton (X-X) interactions with elastic scattering for $\bar{\mathbf{Q}} = 0$ only. Focusing on low-density regime, the X-X interaction between $\mathcal{X}^{\bar{\beta}\dagger}$ and $\mathcal{X}^{\bar{\alpha}\dagger}_{\sigma}$ with states $\bar{\alpha}$ and $\bar{\beta}$ can be calculated from the total energy of the two-exciton state within the same valley $\Omega^{\bar{\beta}\bar{\alpha}}_{\sigma} = \langle 0 | \mathcal{X}^{\bar{\alpha}}_{\sigma} \mathcal{X}^{\bar{\beta}}_{\sigma} \mathcal{H} \mathcal{X}^{\bar{\beta}\dagger}_{\sigma} \mathcal{X}^{\bar{\alpha}\dagger}_{\sigma} | 0 \rangle = \mathcal{E}^{\bar{\beta}}_{\sigma} + \mathcal{E}^{\bar{\alpha}}_{\sigma} + \Delta^{\bar{\beta}\bar{\alpha}}_{\sigma}$. The interacting potential energy is given by

$$\Delta^{\bar{\beta}\,\bar{\alpha}}_{\sigma} = \sum_{\nu\nu'} \sum_{\tilde{\nu}\tilde{\nu}'} \bar{C}^{\bar{\beta}}_{\nu'\sigma} \bar{C}^{\bar{\alpha}}_{\tilde{\nu}'\sigma} C^{\bar{\beta}}_{\nu\sigma} C^{\bar{\alpha}}_{\tilde{\nu}\sigma} \delta_{\tilde{\mathbf{g}}'+\mathbf{g}',\tilde{\mathbf{g}}+\mathbf{g}} \times \left[U^{\nu'\tilde{\nu}'}_{\nu\tilde{\nu}} + U^{\tilde{\nu}'\nu'}_{\nu\tilde{\nu}} - V^{\nu'\tilde{\nu}'}_{\nu\tilde{\nu}} - V^{\tilde{\nu}'\nu'}_{\nu\tilde{\nu}} \right], \tag{9}$$

where the direct [36] and exchange interactions [54] are

$$U^{\nu'\tilde{\nu}'}_{\nu\tilde{\nu}} = \sum_{\mathbf{k}\tilde{\mathbf{k}}\mathbf{q}} \Gamma^{\nu'\tilde{\nu}'}_{\nu\tilde{\nu}}(\mathbf{k}\tilde{\mathbf{k}}, \mathbf{q}) \delta_{\ell_c \ell'_c} \delta_{\ell_v \ell'_v} \delta_{\ell_c \ell'_c} \delta_{\ell_v \ell'_v} \delta_{\mathbf{q},\boldsymbol{g}'-\boldsymbol{g}},$$

$$V^{\nu'\tilde{\nu}'}_{\nu\tilde{\nu}} = \sum_{\mathbf{k}\tilde{\mathbf{k}}\mathbf{q}} \Gamma^{\nu'\tilde{\nu}'}_{\nu\tilde{\nu}}(\mathbf{k}\tilde{\mathbf{k}}, \mathbf{q}) \delta_{\ell_c \ell'_c} \delta_{\ell_v \ell'_v} \delta_{\ell_c \ell'_c} \delta_{\ell_v \ell'_v} \delta_{\mathbf{q},\boldsymbol{g}'-\boldsymbol{g}+\mathbf{k}-\tilde{\mathbf{k}}},$$

that are depicted in Fig. 1(d). Here, $\mathbf{q}$ is the transferred momentum between $\bar{\alpha}$ and $\bar{\beta}$ exciton and the scattering potential is $\Gamma^{\nu'\tilde{\nu}'}_{\nu\tilde{\nu}}(\mathbf{k}\tilde{\mathbf{k}}, \mathbf{q}) = \sum_{\ell\ell'} f^{\ell}_{\nu\sigma}(\mathbf{k}, \mathbf{q}) [v_{\ell\ell'}(\mathbf{q})/2L^2] f^{\ell'}_{\tilde{\nu}\sigma}(\tilde{\mathbf{k}}, -\mathbf{q}) \phi^{*}_{\nu'}(\mathbf{k}) \phi^{*}_{\tilde{\nu}'}(\tilde{\mathbf{k}})$, with the excitonic wave function being expressed in ν-index notation as $\phi_{\nu\sigma}(\mathbf{k}) = \phi^{s}_{\alpha\sigma}(\mathbf{k} - m^{c}_{\ell_c}/M_s \boldsymbol{g})$, and the factor $f^{\ell}_{\nu\sigma}(\mathbf{k}, \mathbf{q}) = \delta_{\ell_c \ell} \phi_{\nu\sigma}(\mathbf{k} - \mathbf{q}) - \delta_{\ell_v \ell} \phi_{\nu\sigma}(\mathbf{k})$. The calculation of the direct interaction $U^{\nu'\tilde{\nu}'}_{\nu\tilde{\nu}}$ is straightforward while evaluating the exchange interaction $V^{\nu'\tilde{\nu}'}_{\nu\tilde{\nu}}$ is rather involved and is detailed in Supplemental Material [53]. We remark that, the result in Eq. (9) is for intravalley interaction and only valid for the low-density regime.

Moiré exciton polariton—Embedding the moiré bilayer into an optical microcavity, excitons can couple strongly to cavity photons, forming polaritonic states. This is an essential mechanism for studying optical nonlinearity [55,56]. Here, dipolar polaritons in GaAs double quantum wells serve as an inspiration for studying pronounced nonlinear effects [57–60]. To study moiré polaritons, we introduce light-matter coupling as an additional term in the system Hamiltonian corresponding to $\mathcal{H}_{\mathrm{sc}} = \sum_{\ell} d^{\ell}_{cv} \sum_{\mathbf{kQ}} c^{\dagger}_{\mathbf{Q}} a^{\dagger}_{\ell\mathbf{k}} b_{\ell\mathbf{k}+\mathbf{Q}} + \mathrm{H.c.} = \sum_{\bar{\alpha}\bar{\mathbf{Q}}} g^{\bar{\alpha}}_{c}(\bar{\mathbf{Q}}) c^{\dagger}_{\bar{\mathbf{Q}}} \mathcal{X}^{\bar{\alpha}}(\bar{\mathbf{Q}}) + \mathrm{H.c.}$ Here $c^{\dagger}_{\mathbf{Q}}$ is the photonic field operator, and d^{ℓ}_{cv} is the interband transition matrix element in ℓ th layer. In the equation, this coupling term is written in the hybridized excitonic basis with coupling constant $g^{\bar{\alpha}}_{c}(\bar{\mathbf{Q}}) = \sum_{\ell\alpha\mathbf{k}} d^{\ell}_{cv} \phi^{\ell\ell}_{\alpha}(\mathbf{k}) \bar{C}^{\bar{\alpha},\ell\ell}_{\alpha\sigma}(\bar{\mathbf{Q}})$.

We consider $\bar{\mathbf{Q}} = 0$ exciton states being dominant as large-$\bar{\mathbf{Q}}$ modes are decoupled from light [61]. Using $\mathcal{H}_{\mathrm{sc}}$ and assuming the exciton in Eq. (3) being a boson described by the operator $\mathcal{X}^{\bar{\alpha}}_{\sigma}(0) \to \hat{x}_{\bar{\alpha}\sigma}$, the photon-cavity coupled system can be written as

$$\mathcal{H}_{\mathrm{xp}} = \omega_c c^{\dagger}_0 c_0 + \sum_{\bar{\alpha}} \left(\mathcal{E}^{\bar{\alpha}}_{\sigma} + \frac{1}{L^2} g^{\bar{\alpha}}_{X} \hat{x}^{\dagger}_{\bar{\alpha}\sigma} \hat{x}_{\bar{\alpha}\sigma} \right) \hat{x}^{\dagger}_{\bar{\alpha}\sigma} \hat{x}_{\bar{\alpha}\sigma} + \mathcal{H}_{\mathrm{sc}}, \tag{10}$$

where the X-X interaction is $g^{\bar{\alpha}}_{X} \approx L^2 \Delta^{\bar{\alpha}\,\bar{\alpha}}$. The exciton-photon interaction is $g^{\bar{\alpha}}_{c} = \frac{1}{2} \sum_{\alpha\ell} \Omega^{\ell}_{\alpha} \bar{C}^{\bar{\alpha},\ell\ell}_{\alpha\sigma}$, where $\Omega^{\ell}_{\alpha} = 2 \sum_{\mathbf{k}} d^{\ell}_{cv} \phi^{\ell\ell}_{\alpha}(\mathbf{k})$ is the Rabi splitting of the exciton in the ℓ th layer and state α.

Result and discussion—To demonstrate the tunability of moiré polaritons described by Eq. (10), we investigate the band hybridization effects for a MoS_2 bilayer marginally twisted from antiparallel stacking or H-type ($\theta \approx 60°$) encapsulated by hexagonal boron nitride ($\epsilon = 4$). We adopt the band parameters from Ref. [62] and use interlayer hoppings of $t_c(\mathbf{K}_{\ell}) = 2.1$ and $t_v(\mathbf{K}_{\ell}) = 14.5$ meV [52]. Using the Gaussian basis function expansion [49,63,64], we solve Eqs. (4) and (7) by keeping only the $1s$ exciton, and plot the θ dependence of exciton energies $\mathcal{E}^{\bar{\alpha}}_{\sigma}$ in Fig. 2(a). The corresponding strength of nonlinearity $g^{\bar{\alpha}}_{X}$

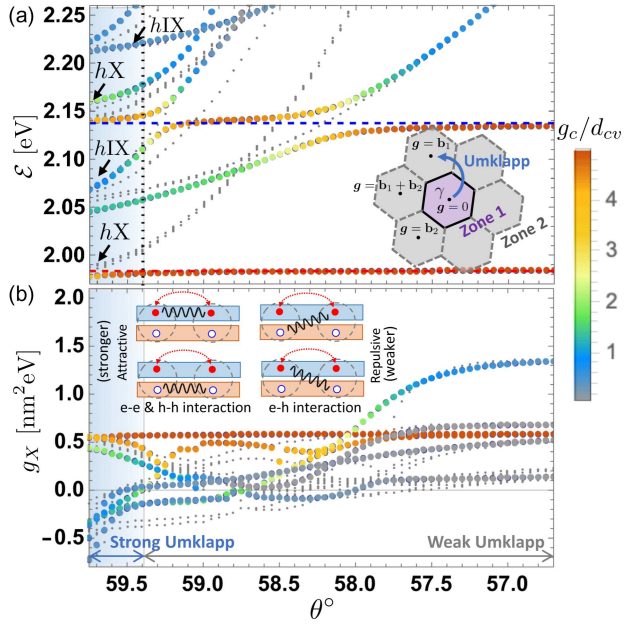

FIG. 2. (a) Exciton energy $\mathcal{E}(\sigma = \uparrow)$ and twisting angle θ dependence. The points are color coded by its light-matter coupling strength g_c. The hybridized excitons weakly interact with light are shown in gray dots. The red and blue dashed lines are the A and B exciton energy with $\theta = 60°$. The vertical dashed line is given by $(\Delta\mathbf{K}^2/2m_v) = t_v$ where the energy separation between folded bands is comparable to interlayer tunneling energy (Inset) the moiré exciton spectrum is calculated by considering the Umklapp scattering that hybridizes the exciton in zone 1 (purple area) and zone 2 (gray area). In the weak Umklapp region, the interlayer and intralayer exciton hybridized with each mBZ separately. (b) θ dependence of the exciton-exciton interaction. (Inset) the interaction (wavy black curves) between interlayer excitons with electron exchange (red dashed curves).

is shown in Fig. 2(b). In the plots each point corresponds to moiré excitons with an associated index $\bar{\alpha}$, and their light-matter coupling strength ($g_c^{\bar{\alpha}}$) is color coded. In Fig. 2(a), we can see two lower branches of bright excitonic modes that correspond to the *hybridized* intralayer exciton hX ($\mathcal{E} \approx 1.98$ eV) and *hybridized* interlayer exciton hIX ($\mathcal{E} \approx 2.05$ eV). These results match previous calculations for single-particle properties discussed in Ref. [51].

In our analysis, we focus on the nonlinear response and X-X interaction strength shown in Fig. 2(b). In the plot we keep only the dominant contributions from Eq. (9) with $\boldsymbol{g}' = \boldsymbol{g}$ for simplicity, since the Coulomb scattering processes with nonzero momentum transfer between the excitons are rapidly suppressed as $\theta \gtrsim 0.5°$. First of all, we find an enhancement in the nonlinear interaction at the small-θ regime indicating the strong influence of the band hybridization due to the umklapp processes. We find strong attractive nonlinearity for hIX while the nonlinear interaction for hX remains repulsive. Intriguingly, these results correlate with measurements in MoS_2 bilayers, where redshifts were observed [30]. The emergence of attractive nonlinearity may be understood as a manifestation of strong anisotropic nature of 2D bilayers. This leads to a weaker interlayer *e-h* interaction as compared to the intralayer *e-e* and *h-h* interaction [Fig. 2(b), inset]. Hence, the total nonlinearity from each of these interacting channels does not cancel leading to stronger attractive nonlinearity. This is different from the monolayer exciton where large cancellations [63–65] between these channels result in a weaker repulsive nonlinearity (~0.5 nm^2 eV). This anisotropic electronic property is unique for 2D materials that enable the realization of attractive interaction between dipolar excitons.

We also note that the strong attractive X-X interaction between hIX in the small θ regime comes from the exchange scattering involving the excitonic modes in Zone 2 [Fig. 2(a), inset]. For instance, in the scattering processes with $\boldsymbol{g} \neq \tilde{\boldsymbol{g}}$ [Fig. 1(d)], the second term in the last line in Eq. (9) (all particle exchange process, repulsive) is strongly suppressed due to large momentum transfer ($\mathbf{q} = \boldsymbol{g} - \tilde{\boldsymbol{g}}$), while the exchange interaction $V_{\nu\tilde{\nu}}^{\nu'\tilde{\nu}'}$ and $V_{\nu\tilde{\nu}}^{\tilde{\nu}'\nu'}$ remain large. This makes a striking difference between moiré bilayer and untwisted bilayer ($\theta = 0$ and 60°) where the scattering processes only take place within Zone 1 with $\boldsymbol{g} = \tilde{\boldsymbol{g}} = 0$. Furthermore, in our calculation, we find weak repulsive direct interaction for hIX in a homobilayer with $\theta \approx 0$ (see Supplemental Material [53]). This may be expected since a large electrical dipole moment is forbidden due to the approximate inversion symmetry. As a result, the dominant contribution to g_X in Fig. 2(b) comes from the (attractive) exchange interactions. However, this can change for heterobilayers or electrically biased samples.

In the presence of electric field $\mathbf{E}_z$, the dipole moment of the interlayer exciton couples to $\mathbf{E}_z$ giving rise to the energy Stark shift. This changes the hybridization content of hX and hIX leading to electrically tunable optical properties. The Stark effect can be incorporated into Eq. (7) by modifying the interlayer exciton energy $E_{\nu\sigma}(\bar{\mathbf{Q}}) \to E_{\nu\sigma}(\bar{\mathbf{Q}}) + \mathbf{E}_z \cdot \boldsymbol{\mu}^s$, where the dipole moment $\boldsymbol{\mu}^s = \pm\mu_z\hat{\mathbf{z}}$ for interlayer exciton with $\mu_z \sim 5$ eÅ [29,66], and $\mu_z = 0$ for intralayer exciton. In Figs. 3(a) and 3(b), we calculate the absorption $\Gamma(\mathcal{E})$. In $\Gamma(\mathcal{E})$, we also take into account the nonlinear energy shift due to the background excitons with density $n_{\bar{\alpha}} = \langle \hat{x}_{\bar{\alpha}\sigma}^\dagger \hat{x}_{\bar{\alpha}\sigma} \rangle / L^2$ (pump-power dependent) [53]. In Fig. 3(a), two brightest branches independent of E_z correspond to the *hybridized A* and *B* intralayer excitons. The other dimmer branches with strong response to E_z are the hIXs. Following one hIX branch indicated by the red and blue dots in Figs. 3(a) and 3(b), we can see that the absorption peaks are enhanced as the hIX approaches the hX branches since hIX gains more intralayer exciton component. Furthermore, we also observe that the hIX nonlinear redshift turns into a blueshift as E_z changes. This is partly due to the repulsive nonlinearity from the intralayer exciton component, and another

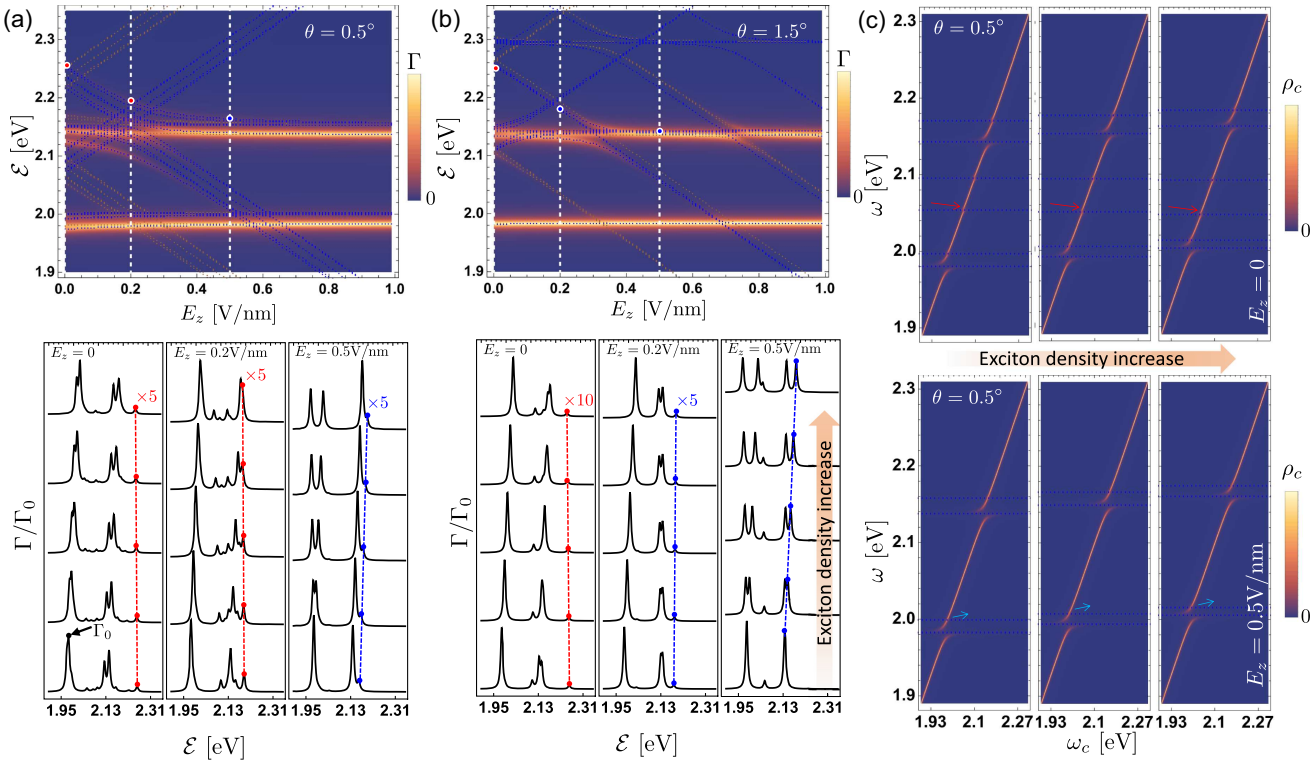

FIG. 3. Upper panel is E_z-field dependence of the *hybridized* moiré exciton absorption spectrum with twisting angles (a) $\theta = 0.5°$ and (b) $\theta = 1.5°$ (normalized by Γ_0). The blue ($\sigma = \uparrow$) and red ($\sigma = \downarrow$) dashed curves highlight the moiré excitonic modes. Lower panel shows the nonlinear spectrum of the power-dependent absorption with $E_z = 0, 0.2, 0.5$ V/nm indicated by the cut (white dashed lines) in the upper panel. Red (blue) dashed lines illustrate the red (blue) shift of the *hybridized* interlayer exciton. (c) Nonlinear polariton spectrum for $\theta = 0.5°$ with $\sigma = \uparrow$. In this plot, we let $\kappa = 1$ and $\gamma_{\tilde{\alpha}} = 3$ meV.

contribution is coming from the polarization of hIX in the high-field regime. These results in Figs. 2 and 3 demonstrate that the nonlinear optical response of moiré material is electrically tunable.

Next, we plot the polaritonic spectrum in Fig. 3(c) by evaluating the photonic density of states $\rho_c(\omega)$ of Eq. (10), which is proportional to the cavity transmission [53]. Tuning the hIX energy closer to the hX energy at $E_z = 0.5$ eV/nm, we enhance the light-matter coupling of hIX leading to the larger Rabi splitting. This also changes the hIX attractive nonlinearity (red arrows) at $E_z = 0$ to a repulsive nonlinearity (blue arrows) with blueshift at $E_z = 0.5$ V/nm.

Conclusion—We developed a microscopic theory for *hybridized* moiré excitons in twisted bilayers. We revealed that hybridization between layers can enhance significantly the nonlinearity of moiré excitons and polaritons, stemming from umklapp processes for small twisting angles. Intriguingly, we find attractive nonlinear interaction for hIX, which can be tuned into repulsive by applying an external electric field. This makes moiré polariton lattices at small twisting angles an excellent platform for studying many-body effects.

Note that in this study we limited ourselves to not-too-large θ regime, since the hybridization between folded bands in the mini Brillouin zone is weak. On the other hand, we do not investigate $\theta \lesssim 0.5°$, as this is typically prevented by the lattice reconstruction [67–71] and also requires accounting for more Umklapp scatterings beyond those pictured in Fig. 2(a). We also stress that the nonlinear properties in our study are valid for low density regimes, and studying higher-order correction is an interesting avenue for future research. This will allow describing a crossover to the strongly correlated regime close to the metal-insulator transition [72–75].

Acknowledgments—We acknowledge the support from UK EPSRC Awards No. EP/X017222/1. K. W. S. is supported by Xiamen University Malaysia Research Fund (Grant No. XMUMRF/2025-C15/IPHY/0005).

[1] L. Balents, C. R. Dean, D. K. Efetov, and A. F. Young, Superconductivity and strong correlations in moiré flat bands, Nat. Phys. **16**, 725 (2020).

[2] S. Carr, S. Fang, and E. Kaxiras, Electronic-structure methods for twisted moiré layers, Nat. Rev. Mater. **5**, 748 (2020).

[3] J. Bloch, A. Cavalleri, V. Galitski, M. Hafezi, and A. Rubio, Strongly correlated electron–photon systems, Nature (London) **606**, 41 (2022).

[4] Y. Cao, V. Fatemi, S. Fang, K. Watanabe, T. Taniguchi, E. Kaxiras, and P. Jarillo-Herrero, Unconventional superconductivity in magic-angle graphene superlattices, Nature (London) **556**, 43 (2018).

[5] F. Wu, T. Lovorn, E. Tutuc, and A. H. MacDonald, Hubbard model physics in transition metal dichalcogenide moiré bands, Phys. Rev. Lett. **121**, 026402 (2018).

[6] Y. Tang, L. Li, T. Li, Y. Xu, S. Liu, K. Barmak, K. Watanabe, T. Taniguchi, A. H. MacDonald, J. Shan, and K. F. Mak, Simulation of Hubbard model physics in WSe_2/WS_2 moiré superlattices, Nature (London) **579**, 353 (2020).

[7] E. C. Regan, D. Wang, C. Jin, M. I. Bakti Utama, B. Gao, X. Wei, S. Zhao, W. Zhao, Z. Zhang, K. Yumigeta, M. Blei, J. D. Carlström, K. Watanabe, T. Taniguchi, S. Tongay, M. Crommie, A. Zettl, and F. Wang, Mott and generalized Wigner crystal states in WSe_2/WS_2 moiré superlattices, Nature (London) **579**, 359 (2020).

[8] F. Wu, T. Lovorn, and A. H. MacDonald, Theory of optical absorption by interlayer excitons in transition metal dichalcogenide heterobilayers, Phys. Rev. B **97**, 035306 (2018).

[9] K. Tran *et al.*, Evidence for moiré excitons in van der Waals heterostructures, Nature (London) **567**, 71 (2019).

[10] K. Tran, J. Choi, and A. Singh, Moiré and beyond in transition metal dichalcogenide twisted bilayers, 2D Mater. **8**, 022002 (2021).

[11] A. J. Campbell, V. Vitale, M. Brotons-Gisbert, H. Baek, A. Borel, T. V. Ivanova, T. Taniguchi, K. Watanabe, J. Lischner, and B. D. Gerardot, The interplay of field-tunable strongly correlated states in a multi-orbital moiré system, Nat. Phys. **20**, 589 (2024).

[12] S. M. Shinde, K. P. Dhakal, X. Chen, W. S. Yun, J. Lee, H. Kim, and J.-H. Ahn, Stacking-controllable interlayer coupling and symmetric configuration of multilayered MoS_2, NPG Asia Mater. **10**, e468 (2018).

[13] Z. Li, J. Förste, K. Watanabe, T. Taniguchi, B. Urbaszek, A. S. Baimuratov, I. C. Gerber, A. Högele, and I. Bilgin, Stacking-dependent exciton multiplicity in WSe_2 bilayers, Phys. Rev. B **106**, 045411 (2022).

[14] K. L. Seyler, P. Rivera, H. Yu, N. P. Wilson, E. L. Ray, D. G. Mandrus, J. Yan, W. Yao, and X. Xu, Signatures of moiré-trapped valley excitons in $MoSe_2/WSe_2$ heterobilayers, Nature (London) **567**, 66 (2019).

[15] L. Zhang, Z. Zhang, F. Wu, D. Wang, R. Gogna, S. Hou, K. Watanabe, T. Taniguchi, K. Kulkarni, T. Kuo, S. R. Forrest, and H. Deng, Twist-angle dependence of moiré excitons in $WS_2/MoSe_2$ heterobilayers, Nat. Commun. **11**, 5888 (2020).

[16] I. Paradisanos, Andres Manuel Saiz Raven, T. Amand, C. Robert, P. Renucci, K. Watanabe, T. Taniguchi, I. C. Gerber, X. Marie, and B. Urbaszek, Second harmonic generation control in twisted bilayers of transition metal dichalcogenides, Phys. Rev. B **105**, 115420 (2022).

[17] V. Villafañe, M. Kremser, R. Hübner, M. M. Petrić, N. P. Wilson, A. V. Stier, K. Müller, M. Florian, A. Steinhoff, and J. J. Finley, Twist-dependent intra-interlayer excitons in moiré $MoSe_2$ homobilayers, Phys. Rev. Lett. **130**, 026901 (2023).

[18] A. Tartakovskii, Moiré or not, Nat. Mater. **19**, 581 (2020).

[19] D. Huang, J. Choi, C.-K. Shih, and X. Li, Excitons in semiconductor moiré superlattices, Nat. Nanotechnol. **17**, 227 (2022).

[20] M. Kögl, P. Soubelet, M. Brotons-Gisbert, A. V. Stier, B. D. Gerardot, and J. J. Finley, Moiré straintronics: A universal platform for reconfigurable quantum materials, npj 2D Mater. Appl. **7**, 32 (2023).

[21] X. Sun, M. Suriyage, A. R. Khan, M. Gao, J. Zhao, B. Liu, M. M. Hasan, S. Rahman, R.-s. Chen, P. K. Lam, and Y. Lu, Twisted van der Waals quantum materials: Fundamentals, tunability, and applications, Chem. Rev. **124**, 1992 (2024).

[22] J. Klein, J. Wierzbowski, A. Steinhoff, M. Florian, M. Rösner, F. Heimbach, K. Müller, F. Jahnke, T. O. Wehling, J. J. Finley, and M. Kaniber, Electric-field switchable second-harmonic generation in bilayer MoS_2 by inversion symmetry breaking, Nano Lett. **17**, 392 (2017).

[23] H. Yu and W. Yao, Electrically tunable topological transport of moiré polaritons, Sci. Bull. **65**, 1555 (2020).

[24] Y. Tang, J. Gu, S. Liu, K. Watanabe, T. Taniguchi, J. Hone, K. F. Mak, and J. Shan, Tuning layer-hybridized moiré excitons by the quantum-confined stark effect, Nat. Nanotechnol. **16**, 52 (2021).

[25] L. Sponfeldner, N. Leisgang, S. Shree, I. Paradisanos, K. Watanabe, T. Taniguchi, C. Robert, D. Lagarde, A. Balocchi, X. Marie, I. C. Gerber, B. Urbaszek, and R. J. Warburton, Capacitively and inductively coupled excitons in bilayer MoS_2, Phys. Rev. Lett. **129**, 107401 (2022).

[26] S. Kovalchuk, K. Greben, A. Kumar, S. Pessel, K. Watanabe, T. Taniguchi, D. Christiansen, M. Selig, A. Knorr, and K. I. Bolotin, Interlayer excitons in semiconductor bilayers under a strong electric field, arXiv:2303.09931.

[27] I. C. Gerber, E. Courtade, S. Shree, C. Robert, T. Taniguchi, K. Watanabe, A. Balocchi, P. Renucci, D. Lagarde, X. Marie, and B. Urbaszek, Interlayer excitons in bilayer MoS_2 with strong oscillator strength up to room temperature, Phys. Rev. B **99**, 035443 (2019).

[28] I. Paradisanos, S. Shree, A. George, N. Leisgang, C. Robert, K. Watanabe, T. Taniguchi, R. J. Warburton, A. Turchanin, X. Marie, I. C. Gerber, and B. Urbaszek, Controlling interlayer excitons in MoS_2 layers grown by chemical vapor deposition, Nat. Commun. **11**, 2391 (2020).

[29] N. Peimyoo, T. Deilmann, F. Withers, J. Escolar, D. Nutting, T. Taniguchi, K. Watanabe, A. Taghizadeh, M. F. Craciun, K. S. Thygesen, and S. Russo, Electrical tuning of optically active interlayer excitons in bilayer MoS_2, Nat. Nanotechnol. **16**, 888 (2021).

[30] C. Louca, A. Genco, S. Chiavazzo, T. P. Lyons, S. Randerson, C. Trovatello, P. Claronino, R. Jayaprakash, X. Hu, J. Howarth, K. Watanabe, T. Taniguchi, S. Dal Conte, R. Gorbachev, D. G. Lidzey, G. Cerullo, O. Kyriienko, and A. I. Tartakovskii, Interspecies exciton interactions lead to enhanced nonlinearity of dipolar excitons and polaritons in MoS_2 homobilayers, Nat. Commun. **14**, 3818 (2023).

[31] L. Zhang, F. Wu, S. Hou, Z. Zhang, Y.-H. Chou, K. Watanabe, T. Taniguchi, S. R. Forrest, and H. Deng,

Van der waals heterostructure polaritons with moiré-induced nonlinearity, Nature (London) **591**, 61 (2021).
[32] B. Datta, M. Khatoniar, P. Deshmukh, F. Thouin, R. Bushati, S. De Liberato, S. K. Cohen, and V. M. Menon, Highly nonlinear dipolar exciton-polaritons in bilayer MoS_2, Nat. Commun. **13**, 6341 (2022).
[33] M. Kremser, M. Brotons-Gisbert, J. Knörzer, J. Gückelhorn, M. Meyer, M. Barbone, A. V. Stier, B. D. Gerardot, K. Müller, and J. J. Finley, Discrete interactions between a few interlayer excitons trapped at a $MoSe_2$–WSe_2 heterointerface, npj 2D Mater. Appl. **4**, 8 (2020).
[34] Q. Hu, Z. Zhan, H. Cui, Y. Zhang, F. Jin, X. Zhao, M. Zhang, Z. Wang, Q. Zhang, K. Watanabe, T. Taniguchi, X. Cao, W.-M. Liu, F. Wu, S. Yuan, and Y. Xu, Observation of Rydberg moiré excitons, Science **380**, 1367 (2023).
[35] J. M. Fitzgerald, J. J. P. Thompson, and E. Malic, Twist angle tuning of moiré exciton polaritons in van der waals heterostructures, Nano Lett. **22**, 4468 (2022).
[36] D. Erkensten, S. Brem, R. Perea-Causín, J. Hagel, F. Tagarelli, E. Lopriore, A. Kis, and E. Malic, Electrically tunable dipolar interactions between layer-hybridized excitons, Nanoscale **15**, 11064 (2023).
[37] Y. Shimazaki, I. Schwartz, K. Watanabe, T. Taniguchi, M. Kroner, and A. Imamoğlu, Strongly correlated electrons and hybrid excitons in a moiré heterostructure, Nature (London) **580**, 472 (2020).
[38] H. Baek, M. Brotons-Gisbert, A. Campbell, V. Vitale, J. Lischner, K. Watanabe, T. Taniguchi, and B. D. Gerardot, Optical read-out of coulomb staircases in a moiré superlattice via trapped interlayer trions, Nat. Nanotechnol. **16**, 1237 (2021).
[39] M. Zimmerman, R. Rapaport, and S. Gazit, Collective interlayer pairing and pair superfluidity in vertically stacked layers of dipolar excitons, Proc. Natl. Acad. Sci. U.S.A. **119**, e2205845119 (2022).
[40] A. J. Campbell, M. Brotons-Gisbert, H. Baek, V. Vitale, T. Taniguchi, K. Watanabe, J. Lischner, and B. D. Gerardot, Exciton-polarons in the presence of strongly correlated electronic states in a $MoSe_2/WSe_2$ moiré superlattice, npj 2D Mater. Appl. **6**, 79 (2022).
[41] T.-S. Huang, P. Lunts, and M. Hafezi, Nonbosonic moiré excitons, Phys. Rev. Lett. **132**, 186202 (2024).
[42] K. W. Song, S. Chiavazzo, and O. Kyriienko, Microscopic theory of nonlinear phase space filling in polaritonic lattices, Phys. Rev. Res. **6**, 023033 (2024).
[43] A. Camacho-Guardian and N. R. Cooper, Moiré-induced optical nonlinearities: Single- and multiphoton resonances, Phys. Rev. Lett. **128**, 207401 (2022).
[44] H. Wang, H. Kim, D. Dong, K. Shinokita, K. Watanabe, T. Taniguchi, and K. Matsuda, Quantum coherence and interference of a single moiré exciton in nano-fabricated twisted monolayer semiconductor heterobilayers, Nat. Commun. **15**, 4905 (2024).
[45] D. Thureja, A. Imamoglu, T. Smoleński, I. Amelio, A. Popert, T. Chervy, X. Lu, S. Liu, K. Barmak, K. Watanabe, T. Taniguchi, D. J. Norris, M. Kroner, and P. A. Murthy, Electrically tunable quantum confinement of neutral excitons, Nature (London) **606**, 298 (2022).
[46] J. Hu, E. Lorchat, X. Chen, K. Watanabe, T. Taniguchi, T. F. Heinz, P. A. Murthy, and T. Chervy, Quantum control of exciton wave functions in 2d semiconductors, Sci. Adv. **10**, eadk6369 (2024).
[47] A. Steinhoff, E. Wietek, M. Florian, T. Schulz, T. Taniguchi, K. Watanabe, S. Zhao, A. Högele, F. Jahnke, and A. Chernikov, Exciton-exciton interactions in van der waals heterobilayers, Phys. Rev. X **14**, 031025 (2024).
[48] S. Latini, T. Olsen, and K. S. Thygesen, Excitons in van der waals heterostructures: The important role of dielectric screening, Phys. Rev. B **92**, 245123 (2015).
[49] A. Ceferino, K. W. Song, S. J. Magorrian, V. Zólyomi, and V. I. Fal'ko, Crossover from weakly indirect to direct excitons in atomically thin films of InSe, Phys. Rev. B **101**, 245432 (2020).
[50] M. Danovich, D. A. Ruiz-Tijerina, R. J. Hunt, M. Szyniszewski, N. D. Drummond, and V. I. Fal'ko, Localized interlayer complexes in heterobilayer transition metal dichalcogenides, Phys. Rev. B **97**, 195452 (2018).
[51] D. A. Ruiz-Tijerina and V. I. Fal'ko, Interlayer hybridization and moiré superlattice minibands for electrons and excitons in heterobilayers of transition-metal dichalcogenides, Phys. Rev. B **99**, 125424 (2019).
[52] Y. Wang, Z. Wang, W. Yao, G.-B. Liu, and H. Yu, Interlayer coupling in commensurate and incommensurate bilayer structures of transition-metal dichalcogenides, Phys. Rev. B **95**, 115429 (2017).
[53] See Supplemental Material at http://link.aps.org/supplemental/10.1103/gr72-szwg for the detailed derivation.
[54] M. Combescot, O. Betbeder-Matibet, and F. Dubin, The many-body physics of composite bosons, Phys. Rep. **463**, 215 (2008).
[55] T. Kuriakose, P. M. Walker, T. Dowling, O. Kyriienko, I. A. Shelykh, P. St-Jean, N. C. Zambon, A. Lemaître, I. Sagnes, L. Legratiet, A. Harouri, S. Ravets, M. S. Skolnick, A. Amo, J. Bloch, and D. N. Krizhanovskii, Few-photon all-optical phase rotation in a quantum-well micropillar cavity, Nat. Photonics **16**, 566 (2022).
[56] M. Makhonin, A. Delphan, K. W. Song, P. Walker, T. Isoniemi, P. Claronino, K. Orfanakis, S. K. Rajendran, H. Ohadi, J. Heckötter, M. Assmann, M. Bayer, A. Tartakovskii, M. Skolnick, O. Kyriienko, and D. Krizhanovskii, Nonlinear Rydberg exciton-polaritons in $\mathbf{Cu_2O}$ microcavities, Light Sci. Appl. **13**, 47 (2024).
[57] I. Rosenberg, D. Liran, Y. Mazuz-Harpaz, K. West, L. Pfeiffer, and R. Rapaport, Strongly interacting dipolar-polaritons, Sci. Adv. **4**, eaat8880 (2018).
[58] E. Togan, H.-T. Lim, S. Faelt, W. Wegscheider, and A. Imamoglu, Enhanced interactions between dipolar polaritons, Phys. Rev. Lett. **121**, 227402 (2018).
[59] O. Kyriienko, I. A. Shelykh, and T. C. H. Liew, Tunable single-photon emission from dipolaritons, Phys. Rev. A **90**, 033807 (2014).
[60] O. Kyriienko and T. C. H. Liew, Exciton-polariton quantum gates based on continuous variables, Phys. Rev. B **93**, 035301 (2016).
[61] G. Wang, A. Chernikov, M. M. Glazov, T. F. Heinz, X. Marie, T. Amand, and B. Urbaszek, Colloquium: Excitons

in atomically thin transition metal dichalcogenides, Rev. Mod. Phys. **90**, 021001 (2018).
[62] A. Kormányos, G. Burkard, M. Gmitra, J. Fabian, V. Zólyomi, N. D. Drummond, and V. Fal'ko, k · p theory for two-dimensional transition metal dichalcogenide semiconductors, 2D Mater. **2**, 022001 (2015).
[63] K. W. Song, S. Chiavazzo, I. A. Shelykh, and O. Kyriienko, Attractive trion-polariton nonlinearity due to Coulomb scattering, arXiv:2204.00594.
[64] K. W. Song, S. Chiavazzo, I. A. Shelykh, and O. Kyriienko, Theory for coulomb scattering of trions in 2d materials, arXiv:2207.02660.
[65] V. Shahnazaryan, I. Iorsh, I. A. Shelykh, and O. Kyriienko, Exciton-exciton interaction in transition-metal dichalcogenide monolayers, Phys. Rev. B **96**, 115409 (2017).
[66] N. Leisgang, S. Shree, I. Paradisanos, L. Sponfeldner, C. Robert, D. Lagarde, A. Balocchi, K. Watanabe, T. Taniguchi, X. Marie, R. J. Warburton, I. C. Gerber, and B. Urbaszek, Giant Stark splitting of an exciton in bilayer MoS_2, Nat. Nanotechnol. **15**, 901 (2020).
[67] M. H. Naik and M. Jain, Ultraflatbands and shear solitons in moiré patterns of twisted bilayer transition metal dichalcogenides, Phys. Rev. Lett. **121**, 266401 (2018).
[68] S. Carr, D. Massatt, S. B. Torrisi, P. Cazeaux, M. Luskin, and E. Kaxiras, Relaxation and domain formation in incommensurate two-dimensional heterostructures, Phys. Rev. B **98**, 224102 (2018).
[69] M. H. Naik, I. Maity, P. K. Maiti, and M. Jain, Kolmogorov–Crespi potential for multilayer transition-metal dichalcogenides: Capturing structural transformations in moirésuperlattices, J. Phys. Chem. C **123**, 9770 (2019).
[70] V. V. Enaldiev, V. Zólyomi, C. Yelgel, S. J. Magorrian, and V. I. Fal'ko, Stacking domains and dislocation networks in marginally twisted bilayers of transition metal dichalcogenides, Phys. Rev. Lett. **124**, 206101 (2020).
[71] A. Weston, Y. Zou, V. Enaldiev, A. Summerfield, N. Clark, V. Zólyomi, A. Graham, C. Yelgel, S. Magorrian, M. Zhou, J. Zultak, D. Hopkinson, A. Barinov, T. H. Bointon, A. Kretinin, N. R. Wilson, P. H. Beton, V. I. Fal'ko, S. J. Haigh, and R. Gorbachev, Atomic reconstruction in twisted bilayers of transition metal dichalcogenides, Nat. Nanotechnol. **15**, 592 (2020).
[72] E. Blundo, F. Tuzi, S. Cianci, M. Cuccu, K. Olkowska-Pucko, Ł. Kipczak, G. Contestabile, A. Miriametro, M. Felici, G. Pettinari, T. Taniguchi, K. Watanabe, A. Babiński, M. R. Molas, and A. Polimeni, Localisation-to-delocalisation transition of moiréexcitons in $WSe_2/MoSe_2$ heterostructures, Nat. Commun. **15**, 1057 (2024).
[73] B. Gao, D. G. Suárez-Forero, S. Sarkar, T.-S. Huang, D. Session, M. J. Mehrabad, R. Ni, M. Xie, P. Upadhyay, J. Vannucci, S. Mittal, K. Watanabe, T. Taniguchi, A. Imamoglu, Y. Zhou, and M. Hafezi, Excitonic mott insulator in a Bose-Fermi-Hubbard system of moiré WS_2/WSe_2 heterobilayer, Nat. Commun. **15**, 2305 (2024).
[74] T.-S. Huang, Y.-Z. Chou, C. L. Baldwin, F. Wu, and M. Hafezi, Mott-moiré excitons, Phys. Rev. B **107**, 195151 (2023).
[75] H. Park, J. Zhu, X. Wang, Y. Wang, W. Holtzmann, T. Taniguchi, K. Watanabe, J. Yan, L. Fu, T. Cao, D. Xiao, D. R. Gamelin, H. Yu, W. Yao, and X. Xu, Dipole ladders with large Hubbard interaction in a moiré exciton lattice, Nat. Phys. **19**, 1286 (2023).